THE JOURNAL OF PHYSICAL CHEMISTRY C

ARTICLE

pubs.acs.org/JPCC

Microwave-Assisted Hydrothermal Synthesis of Nanosized α-Fe_2O_3 for Catalysts and Adsorbents

Guohong Qiu,[†,‡] Hui Huang,[‡] Homer Genuino,[‡] Naftali Opembe,[‡] Lisa Stafford,[‡] Saminda Dharmarathna,[‡] and Steven L. Suib*[,‡]

[†]Key Laboratory of Subtropical Agricultural Resources and Environment, Ministry of Agriculture, College of Resources and Environment, Huazhong Agricultural University, Wuhan 430070, P. R. China

[‡]Department of Chemistry, University of Connecticut, Storrs, 55 North Eagleville Road, Storrs, Connecticut 06269, United States

ABSTRACT: Nanosized α-Fe_2O_3 powder was synthesized by a microwave-assisted hydrothermal reaction of $Fe(NO_3)_3$ and urea at 120 °C for 30 min. The products were characterized by X-ray diffraction, transmission electron microscopy, BET measurements, Fourier transform infrared spectroscopy, and thermogravimetric analysis. The catalytic performance of α-Fe_2O_3 was studied for the oxidation of CO and 2-propanol to CO_2, and the adsorption properties were investigated for the removal of As(III) in water treatment. Uniform α-Fe_2O_3 particles about 5.0 nm in diameter were formed with a surface area of around 173.0 m^2 g^{-1}. When 0.1 g of α-Fe_2O_3 powder worked as a catalyst, CO was oxidized to CO_2 over 120 °C and completely transformed to CO_2 at 170 °C, and 2-propanol was fully oxidized to CO_2 at 350 °C. The adsorption capacity for As(III) reached 51.8 mg g^{-1} at room temperature. This work facilitates the preparation of nanosized α-Fe_2O_3 materials with excellent catalytic and adsorption performance.

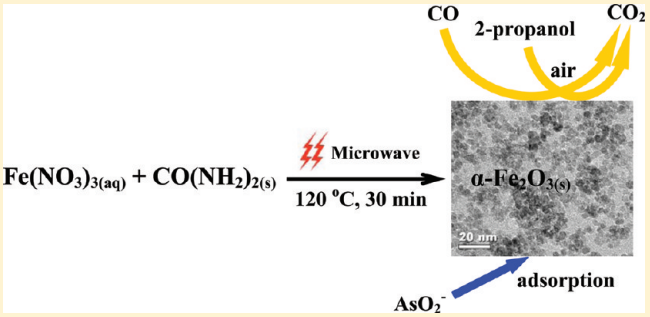

1. INTRODUCTION

Ferric oxides, particularly hematite (α-Fe_2O_3), have drawn significant interest for their potential applications in the field of catalysis,[1−3] as chemical power sources,[4,5] in magnetics,[2,6,7] as sensors,[8] and in water treatment[9−11] due to their unique physical/chemical properties and relatively low cost. The structural morphology and particle size play important roles in determining the functions of α-Fe_2O_3.[12,13] As for magnetic materials, when the single-domain particle becomes small enough, the magnetic moment in the domain fluctuates due to thermal agitation, and superparamagnetic phenomena occur for small particle sizes of α-Fe_2O_3.[13] As electrode materials of secondary lithium-ion batteries, the discharge capacity of α-Fe_2O_3 nanocrystals can be enhanced with an increase in the specific surface area.[4] Hierarchically nanostructured α-Fe_2O_3 hollow spheres assembled by nanosheets exhibited excellent photocatalytic activities. However, their adsorption capacities for As(III) and organic pollutants are limited due to the low specific surface area.[10,14] Ultrafine α-Fe_2O_3 nanoparticles were fabricated with high specific surface area and demonstrated effective performance for the removal of As(III) contaminants.[15] Specific synthetic conditions are needed for controlling the particle sizes and morphologies of α-Fe_2O_3, leading to improved physicochemical properties and novel applications.

Much effort has been devoted to the fabrication of α-Fe_2O_3 nanoparticles and nanofibers. α-Fe_2O_3 nanomaterials can be prepared by calcination of $Fe(OH)_3$ nanotubes at 450 °C, using ZnO as a precursor.[7] Organic iron(II) lactate hydrate has also been used to obtain α-Fe_2O_3 by spray pyrolysis from 600 to 1000 °C.[4] Microwave irradiation and sonochemical syntheses have been conducted to manufacture amorphous ferric oxides that result in crystalline α-Fe_2O_3 after sintering.[2,16] Microwave plasma jets were also used in a multistep process to synthesize Fe_2O_3 with particle sizes of 20−40 nm, where mixed phases were formed, and the crystalline structure could not be controlled.[17] Microwave-assisted hydrolysis of iron salt solutions was performed to synthesize α-Fe_2O_3 only at high Fe^{3+} concentrations and temperatures.[18] In order to reduce energy consumption and simplify procedures, hydrothermal reactions have been performed to directly synthesize lenticular nanorods and dendritic microstructures of magnetic α-Fe_2O_3.[19−21] Microwave-assisted hydrothermal synthesis not only significantly reduces the preparation time from days to minutes but also easily screens a wide range of experimental conditions in order to optimize and scale-up syntheses of such materials with low energy consumption.[22−25]

The α-Fe_2O_3 nanomaterials were prepared using $FeCl_3$ by a microwave-hydrothermal method at 220 °C, and the morphology was controlled by adjusting the concentration of $(NH_4)H_2PO_4$. The reaction conditions needed to be precisely

Received: July 14, 2011
Revised: September 12, 2011
Published: September 13, 2011

dx.doi.org/10.1021/jp2067217 | J. Phys. Chem. C 2011, 115, 19626–19631

controlled. A specific surface area of 75 m^2 g^{-1} was obtained due to particle sizes over 100 nm.[23,24] Ferric salt species and reaction systems might affect the morphologies and particle sizes of α-Fe_2O_3 in the process.[23−25] In order to fully utilize advantages of the microwave-hydrothermal method, lower temperatures and cheaper reagents should be selected to synthesize smaller particles with high specific surface areas, which will increase the potential applications of α-Fe_2O_3.

In recent years, environmental problems, such as air and water pollution, have promoted fundamental and applied research in the area of environmental remediation. Exploiting low-cost catalysts and adsorbents with high performace is an important research focus in this field.

Stream reforming of methanol has been commonly used to generate hydrogen fuel for polyelectrolyte type fuel cells in electric vehicles. However, about 1 vol % CO is usually contained in the hydrogen fuel from the reformers, which is poisonous toward the electrocatalysts of the fuel cells.[26] Catalytic oxidation of CO is not only an important reaction for many applications, such as removal of exhaust gas and in fuel cells, but it is also a fundamental process involving the participation of surface oxygen and oxygen vacancies.[27] The catalytic oxidation of CO to CO_2 in air has attracted much attention since some inexpensive metal oxides, such as Fe_2O_3, can be used to substitute for noble-metal-free and noble-metal-containing oxide catalysts.[1] Quasi-cubic α-Fe_2O_3 nanoparticles were synthesized by a simple solvothermal method and exhibited excellent catalytic performance.[1] In order to evaluate the feasibility for the practical application of the synthesized ferric oxides, the influence of temperature on catalytic activity and the lowest temperature for nanosized α-Fe_2O_3 possessing activity need to be further studied.

Arsenic occurs as a primary highly toxic pollutant in water sources, particularly in groundwater, and arsenic pollution has attracted growing attention.[9] Several treatments have been developed for the removal of As(III) from contaminated water. Among them, adsorption is one of the most effective ways to remove As(III) from water, and superior sorbents need to be selected.[14] Although manganese oxides can be used to effectively remove As(III) from aqueous solution,[28] the costs could be reduced when cheaper adsorbents are selected. Natural zeolites are hydrated aluminosilicate minerals that are abundant, low-cost resources and have been used to remove ammonia and heavy metal ions due to their superior property as ion-exchange materials. However, such zeolites usually have little affinity for anions in aqueous solution due to the net negative charge on the framework.[29] Currently, removal of As(III) using natural zeolites can be achieved on Fe^{3+}-exchanged and surfactant-modified forms; however, the adsorption capacity needs to be further enhanced.[29] Iron oxides and oxy-hydroxides are the most widely used adsorbents for arsenic removal due to their high removal capacity, the strong binding of adsorbed arsenic, and their low cost.[30] Unconventional methods should be performed to further reduce costs and simplify the preparation process of nanosized α-Fe_2O_3.

In this work, nanosized α-Fe_2O_3 was synthesized by a microwave-assisted hydrothermal technique using $Fe(NO_3)_3$ and urea at 120 °C for 30 min. The catalytic oxidation performance for CO and 2-propanol to CO_2 and adsorption properties for the removal of As(III) in water treatment were studied. This approach not only contributes to new synthesis methods for nanosized α-Fe_2O_3 but also provides a new technique for the preparation of other metal oxide nanomaterials.

2. EXPERIMENTAL SECTION

2.1. Preparation and Characterization of α-Fe_2O_3. All reagents used were of analytical grade and purchased from Aldrich, unless otherwise noted. A mixture of 10 mL of 0.1 mol L^{-1} $Fe(NO_3)_3$ and 0.5 mol L^{-1} urea aqueous solution was prepared in a 20 mL reactor vial and then sealed. The apparatus was equipped with a magnetic stirrer. The reactions were carried out in a Biotage Initiator microwave synthesizer, which was programmed to heat up to 120 °C with a holding time from 10 to 30 min. All the synthesized products were washed with distilled deionized water (DDW) several times to remove any possible impurities.

The as-obtained products were characterized with X-ray diffraction (XRD) at room temperature using a Scintag XDS 2000 instrument with Cu Kα radiation. The diffractometer was operated at a tube voltage of 45 kV and a tube current of 40 mA. Fourier transform infrared spectroscopy (FTIR, Nicolet 8700) was carried out with a Bruker Equinox 55 model spectrophotometer by making pellets with KBr powder, and the resolution was set at 4 cm^{-1} with a scan number of 15.

The thermal stability of the products was determined with an SDT Q600 thermogravimetric analysis (TGA) instrument at a heating rate of 4 °C min^{-1}, and TGA analysis was done in an argon atmosphere. The BET surface area of α-Fe_2O_3 powder was tested with a Quantachrome Autosorb-1-C automated N_2 gas adsorption system. A roughly 0.25 g sample was weighed and degassed at 120 °C for 12 h before N_2 physisorption measurements. High-resolution transmission electron microscopy (HR-TEM) experiments were performed using a JEOL 2010 instrument with an accelerating voltage of 200 kV. Before and after catalytic reactions, the α-Fe_2O_3 powders were dispersed in ethanol. A drop of the homogeneous dispersion was loaded on a carbon coated copper grid and allowed to dry before analysis.

2.2. Catalytic Oxidation of CO. The catalytic performance tests were carried out at atmospheric pressure in a quartz tubular fixed bed flow reactor. The temperature of the reactor was monitored using a K-type thermocouple in direct contact with the catalyst upstream of the bed and was regulated with a proportional-integral-derivative (PID) temperature controller. A 100 mg α-Fe_2O_3 sample was used in the experiment. The feed gas was composed of 1% CO, 20% O_2, and 5% N_2 by volume in helium with a space velocity of 35 000 mL h^{-1} g_{cat}^{-1} using mass flow controllers. Nitrogen was included as an internal standard for gas chromatography (GC).

The reaction products were analyzed using an online gas chromatograph [SRI 8610C Gas Chromatograph (GC)] equipped with a 6′ molecular sieve, a 6′ silica gel column, and a thermal conductivity detector (TCD). The carrier gas for the GC was helium. Before each experiment, the catalysts were pretreated by flowing He (50 mL min^{-1}) for 2 h at 120−180 °C. GC samples were injected after 10 min stabilization at any given temperature.

2.3. Gas-Phase Catalytic Oxidation of 2-Propanol. The gas-phase oxidation of 2-propanol to CO_2 using 100 mg of α-Fe_2O_3 catalyst was carried out on a conventional quartz tubular fixed bed flow reactor at atmospheric pressure. The temperature of the reactor was monitored and controlled as above. The catalyst was pretreated by flowing ultrahigh purity helium at a flow rate of 50 mL min^{-1} at 200 °C for 2 h to completely dry and remove any adsorbed species on the catalyst surface. The

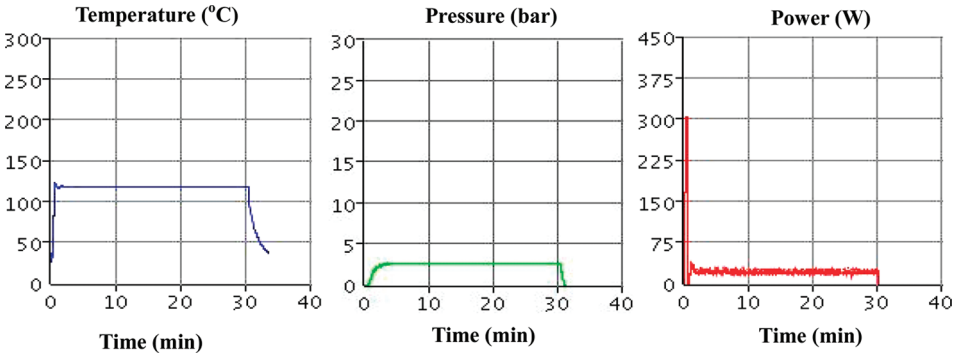

Figure 1. Representative profile of *T*, *P*, and *p* monitored when the reaction was performed at 120 °C, 30 min.

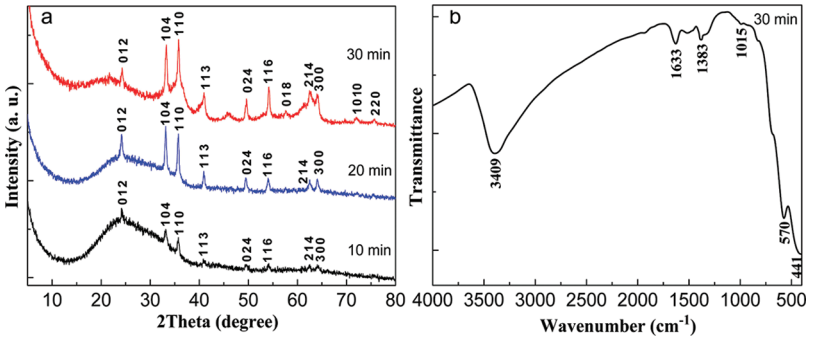

Figure 2. XRD patterns (a) and FTIR spectra (b) of the products synthesized at 120 °C at different times in 0.1 M $Fe(NO_3)_3$ and 0.5 M urea aqueous solutions.

catalytic performance was performed by bubbling ultrahigh pure air (21 vol % O_2) as the feed gas into 200 mL of 2-propanol solution at a flow rate of 20 mL min^{-1} and maintained using mass flow controllers. The reaction was carried out at 100−400 °C. Catalytic data were collected after allowing 20 min stabilization at each analysis temperature. The feed and product gas streams were analyzed using an SRI 8610C gas chromatograph equipped with a 6′ molecular sieve, a 6′ silica gel column, and a thermal conductivity detector (TCD). Helium was used as a carrier gas for all analyses. Since the GC system could not quantify 2-propanol, the percent conversions were calculated in terms of O_2 (limiting reagent) consumption based on peak areas.

2.4. Adsorption of AsO_2^- by α-Fe_2O_3. $NaAsO_2$ (0.3118 g) was dissolved in 2.0 L of 0.1 mol L^{-1} $NaNO_3$ solution, and the AsO_2^- concentration was controlled at 1.2 mmol L^{-1}. Second, 1, 2, 3, 4, 5, 6, 8, 10, 12, 14, 16, 18, and 20 mL $NaAsO_2$ solutions were mixed with 0.1 mol L^{-1} $NaNO_3$ aqueous solution, respectively, keeping the total volume of the mixed solutions at 20 mL. Then, the as-obtained α-Fe_2O_3 powder (about 20.0 mg) was ground and added to the above solutions, respectively. Subsequently, the pH values of the mixtures were adjusted to 7.5 by adding 0.01 mol L^{-1} NaOH and HNO_3 solutions containing 0.1 mol L^{-1} $NaNO_3$. The adsorption reactions were performed in 50 mL polyethylene centrifuge tubes by shaking at 25 ± 1 °C for 24 h and then centrifuged at 8000 rpm for 10 min. The supernatant solutions were collected, and the concentrations of As were measured using inductively coupled plasma atomic emission spectrometry (ICP-AES, Thermo Jarrel Ash).

3. RESULTS AND DISCUSSION

3.1. Preparation and Characterization of α-Fe_2O_3. Figure 1 shows the temperature (*T*), pressure (*P*), and power (*p*) profiles when the reaction was conducted at 120 °C for 30 min. Reaction temperature in the reactor vial was well maintained at 120 °C, the pressure was kept at 2.5 bar, and the power was about 24 W when the reaction proceeded, which indicated that the energy consumption was very low in the process.

Figure 2 shows the powder X-ray diffraction (XRD) patterns and FTIR spectrum of the prepared ferric oxides at different times. The XRD patterns indicate that the products were all α-Fe_2O_3 (JCPDS No. 33-0664). The degree of crystallinity of the products was improved with increased reaction time. Based on these results, the possible formation mechanism for α-Fe_2O_3 was described as follows:

$$CO(NH_2)_{2(s)} + 3H_2O_{(l)} \rightarrow CO_{2(g)} + 2NH_4OH_{(aq)} \quad (1)$$

$$NH_4OH_{(aq)} \rightarrow NH_{4^+(aq)} + OH^-_{(aq)} \quad (2)$$

$$Fe^{3+}_{(aq)} + OH^-_{(aq)} \rightarrow Fe(OH)_{3(s)} \rightarrow \alpha\text{-}Fe_2O_{3(s)} \quad (3)$$

Due to the fact that the product yield was very low at 5 min, the precipitate was not collected. $Fe(OH)_3$ was not observed during the process likely due to a rapid thermal decomposition under microwave heating. In order to increase the yield, the reaction time was set at 30 min, and the product was further characterized by FTIR (Figure 2b). The absorption bands at 441 and 570 cm^{-1}

dx.doi.org/10.1021/jp2067217 |J. Phys. Chem. C 2011, 115, 19626–19631

are attributed to the Fe−O bond vibration. The bands at 1015 and 1383 cm^{-1} correspond to residual hydroxyl groups. The bands at 1633 and 3409 cm^{-1} are assigned to bending modes of water.[31,32]

Although the absorption band at 1383 cm^{-1} attributed to residual hydroxyl groups might come from residual nitrato ions, the absorption bands of NO_3^- were not observed in the FTIR spectrum and there were no diffraction peaks of nitrate in the XRD data, suggesting that pure products were obtained after washing several times with DDW.

The product was further characterized by thermogravimetric analysis (TGA). The TGA curve (Figure 3) shows that the weight loss is about 9.3% and 3.5% from 50 to 1000 °C and from 1000 to 1450 °C, respectively. These weight losses were possibly due to the removal of adsorbed water and thermal decomposition of Fe_2O_3 to Fe_3O_4, respectively.[16] These TGA data are in agreement with the strong absorption bands of water in the FTIR spectrum (Figure 2b).

Figure 4 shows the TEM images, lattice fringes, and selected area electron diffraction (SAED) patterns of the synthesized α-Fe_2O_3. The TEM images show uniform granular crystals about 5.0 nm in size that were formed when the microwave-assisted hydrothermal reaction lasted for 30 min (Figure 4a). The lattice fringes in a typical HRTEM image (Figure 4b) are separated by ~2.5 Å, which agreed well with the {110} lattice spacing of hematite. Continuous sharp rings on the SAED patterns (inset of Figure 4b) further confirmed that the product was α-Fe_2O_3.

Nitrogen gas adsorption measurements were conducted to determine the Brunauer−Emmett−Teller (BET) specific surface area of α-Fe_2O_3. The specific surface area is as high as 173.0 $m^2\ g^{-1}$. The amount adsorbed rose gradually at lower relative pressures and then increased sharply at higher relative pressures as shown in Figure 5. This was in accordance with the characteristics of a type IV isotherm with a type H3 hysteresis loop associated with aggregates (loose assemblages) of platelike particles forming slitlike pores.[9,33] The observed hysteresis loop shifts to a higher relative pressure on approaching $P/P_0 = 1$ (Figure 5), suggesting the presence of macropores and a low degree of aggregation,[9] which was confirmed by TEM images (Figure 4a). The Barrett−Joyner−Halenda (BJH) pore size distribution obtained from the isotherm indicated that most of the pores range from 2 to 20 nm as shown in the inset of Figure 5, which further proved the loose structures and a low degree of aggregation.

3.2. Catalytic Oxidation of CO and 2-Propanol. For catalytic studies in the oxidation of CO, mixed gases (1 vol % CO + 5 vol % N_2 + 20 vol % O_2 + 74 vol % He) flowed through 0.1 g of α-Fe_2O_3 in the bed at different temperatures. Conversion to CO_2

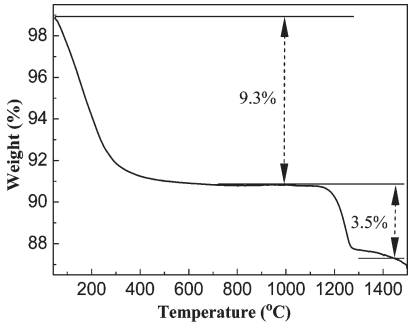

Figure 3. Typical TGA curve of the synthesized α-Fe_2O_3.

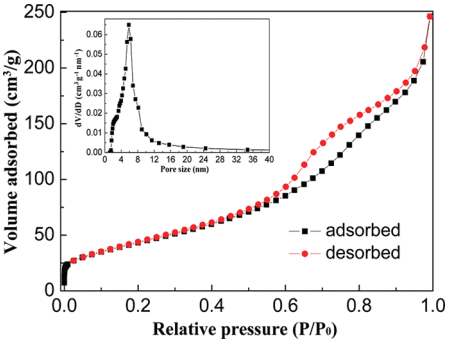

Figure 5. Nitrogen adsorption−desorption isothermal curves of the synthesized α-Fe_2O_3.

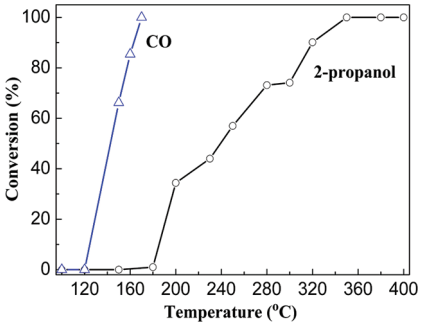

Figure 6. Conversion of CO and 2-propanol to CO_2 oxidized by air using 0.1 g of α-Fe_2O_3 powder under different temperatures.

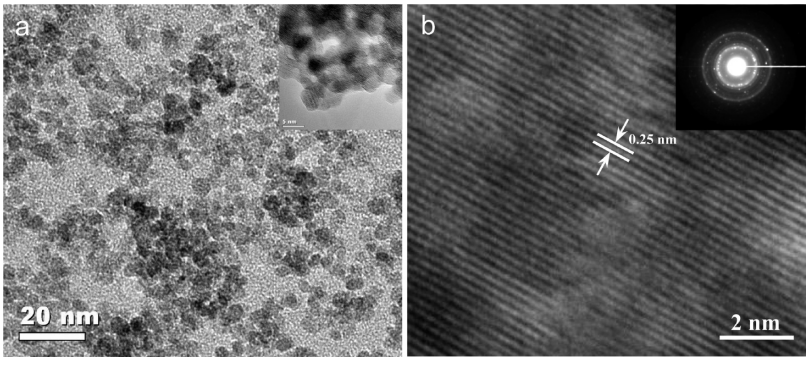

Figure 4. Typical TEM images (a) and HRTEM image (b, with SAED patterns in the inset) of the synthesized α-Fe_2O_3.

dx.doi.org/10.1021/jp2067217 |J. Phys. Chem. C 2011, 115, 19626–19631

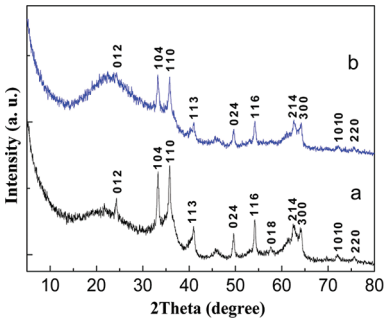

Figure 7. XRD patterns of the synthesized α-Fe_2O_3 before (a) and after (b) 16 h catalytic oxidation of CO to CO_2 at 170 °C.

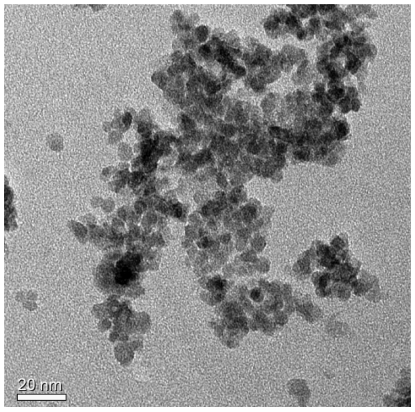

Figure 8. Typical TEM image of α-Fe_2O_3 after catalytic reaction of CO to CO_2 at 170 °C for 16 h.

was zero when the temperature was below 120 °C and increased to 66.2%, 85.4%, and 100.0% at 150, 160, and 170 °C, respectively, at a flow rate of 10 mL min^{-1} (Figure 6).

The conversion remained at 100% after more than 16 h of catalytic oxidation. The conversion decreased from 100% to 79.9% and 65.7% at 170 °C when the flow rates of mixed gases were increased from 10 to 20 and 30 mL min^{-1}, respectively. Increasing the reaction temperature facilitated the oxidation of CO at higher flow rates.[1]

The spent α-Fe_2O_3 catalysts were characterized by XRD to check the stability of the catalyst. After a series of catalytic oxidations of CO to CO_2 from 90 to 170 °C, the experiment was continued for more than 16 h at 170 °C. The crystal structure of α-Fe_2O_3 did not obviously change after reaction (Figure 7), suggesting that α-Fe_2O_3 is a promising catalyst with excellent stability.

The morphologies of the spent α-Fe_2O_3 powder were further characterized by TEM (Figure 8). There was no obvious change in particle size after the catalytic oxidation reaction of CO to CO_2 at 170 °C for 16 h. The α-Fe_2O_3 particles did not form agglomerates after catalytic reaction, indicating that the surface area of the catalyst retained the high specific surface area during reaction.

Catalytic oxidation activity was exhibited when the applied temperature was over 120 °C, which may lead to further applications of α-Fe_2O_3 nanocrystals, such as in gas purification and carbon monoxide gas sensors.

Previous studies have shown that ethanol and 2-propanol could be selectively oxidized to acetaldehyde and acetone,

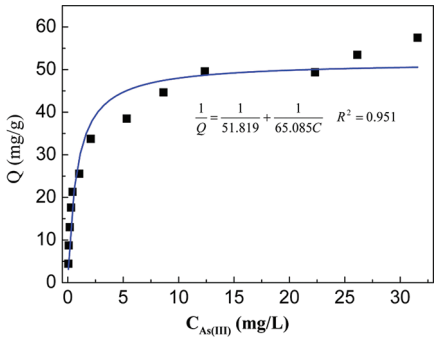

Figure 9. Isotherm of the As(III) adsorption on the synthesized α-Fe_2O_3 with pH 7.5 at 25 °C.

respectively, before CO_2 is formed using metal oxides and noble metal catalysts. High catalytic activities, including total oxidation to CO_2, have also been shown using manganese oxides and nickel foils.[34−36]

A preliminary study of the gas-phase total oxidation of 2-propanol to CO_2 over a α-Fe_2O_3 catalyst was conducted. Ultrahigh purity air (21 vol % O_2) was bubbled into 200 mL of 2-propanol at a flow rate of 20 mL min^{-1} controlled with a mass flow controller. CO_2 was formed at 180 °C (1%), and conversion increased to 34% at 200 °C. Complete conversion of 2-propanol to CO_2 was obtained at 350 °C (Figure 6). The catalytic temperature for the complete transformation into CO_2 was lower than that reported for nickel foils,[35] which suggested that acetone might be formed at a lower temperature. The results also indicated that α-Fe_2O_3 is a potential catalyst for the oxidation of alcohols. Determination of possible intermediates and the reaction mechanism is currently underway.

Most importantly, ferric oxide is much cheaper than nickel and noble metals and noble-metal oxides. These studies clearly show that these α-Fe_2O_3 materials can be used for the oxidation of alcohols, especially for selective catalytic oxidations.

3.3. Removal of As(III). Nanosized α-Fe_2O_3 can be economically used as adsorbents for As(III) removal due to its large specific surface area and low cost. Figure 9 shows the adsorption isotherms of As(III) on synthesized α-Fe_2O_3 nanoparticles at room temperature. When the equilibrium concentration of AsO_2^- was increased from the lowest value, the adsorption amount first increased sharply, then increased slightly, and then tended to remain stable and approached a maximum (Figure 9).

In the present work, the Langmuir equation is used to analyze the data. The Langmuir model is based on several assumptions, including a homogeneous surface, localized adsorption on the surface, and monomolecular occupation of active sites.[10,11,14] The Langmuir isotherm equation may be described as

$$\frac{1}{Q} = \frac{1}{Q_m} + \frac{1}{KQ_mC} \quad (4)$$

where Q is the adsorption capacity of the nanosized α-Fe_2O_3 (mg g^{-1}) at equilibrium, C is the concentration of As(III) in the equilibrium solution (mg L^{-1}), and Q_m is the maximum adsorption capacity (mg g^{-1}). The parameter K is the Langmuir sorption equilibrium constant (L mg^{-1}) related to the free energy of adsorption. The adsorption isotherm fits the Langmuir model with an excellent correlation. The maximum adsorption amount was calculated to be 51.8 mg g^{-1} (691.4 mmol kg^{-1}), which was much larger than those reported by using α-Fe_2O_3

and ZnO,[14,15,37] and better than nanoporous TiO_2 for the removal of As(V).[38] These results indicated that the as-obtained nanosized α-Fe_2O_3 had a larger adsorption capacity for As(III) and could be potentially used as an excellent adsorbent in water treatment.

4. CONCLUSIONS

Nanosized α-Fe_2O_3 has been successfully prepared by a microwave-assisted hydrothermal reaction of $Fe(NO_3)_3$ and urea at 120 °C in aqueous solution for 30 min. The particle size was uniform and about 5.0 nm in diameter. The α-Fe_2O_3 material exhibited excellent catalytic performance for the oxidation of CO and 2-propanol to CO_2 and could be a promising adsorbent for As(III) removal in water treatment. The maximum adsorption capacity for As(III) reached 51.8 mg g^{-1} at room temperature. The nanosized α-Fe_2O_3 synthesized in this work also has potential applications for Li batteries, for magnetic materials, and as sensors, which are now under investigation.

AUTHOR INFORMATION

Corresponding Author

*Tel. 1 860 486 2797; fax 1 860 486 2981.

ACKNOWLEDGMENT

The authors thank the National Natural Science Foundation of China (grant numbers 41171375, 40830527, and 20807019) and the Fundamental Research Funds for the Central Universities (program number 2011PY015) for financial support. We acknowledge the U.S. Department of Energy, Office of Basic Energy Sciences, Division of Chemical, Geochemical and Biological Sciences for support of this work. The authors also gratefully acknowledge Dr. Frank S. Galasso at the University of Connecticut for useful suggestions.

REFERENCES

(1) Zheng, Y. H.; Cheng, Y.; Wang, Y. S.; Bao, F.; Zhou, L. H.; Wei, X. F.; Zhang, Y. Y.; Zheng, Q. *J. Phys. Chem. B* **2006**, *110*, 3093–3097.
(2) Srivastava, D. N.; Perkas, N.; Gedanken, A.; Felner, I. *J. Phys. Chem. B* **2002**, *106*, 1878–1883.
(3) Zhang, P.; Chi, M. F.; Sharma, S.; McFarland, E. *J. Mater. Chem.* **2010**, *20*, 2013–2017.
(4) Chou, S. L.; Wang, J. Z.; Wexler, D.; Konstantinov, K.; Zhong, C.; Liu, H. K.; Dou, S. X. *J. Mater. Chem.* **2010**, *20*, 2092–2098.
(5) Reddy, M. V.; Yu, T.; Sow, C. H.; Shen, Z. X.; Lim, C. T.; Rao, G. V. S.; Chowdari, B. V. R. *Adv. Funct. Mater.* **2007**, *17*, 2792–2799.
(6) Kim, C. H.; Chun, H. J.; Kim, D. S.; Kim, S. Y.; Park, J.; Moon, Je Y.; Lee, G.; Yoon, J.; Jo, Y.; Jung, M. H.; Jung, S.; Lee, C. J. *Appl. Phys. Lett.* **2006**, *89*, 223103.
(7) Wang, Q.; Geng, B. Y.; Wang, S. Z.; Ye, Y. X.; Tao, B. *Chem. Commun.* **2010**, *46*, 1899–1901.
(8) Gou, X. L.; Wang, G. X.; Park, J.; Liu, H.; Yang, J. *Nanotechnology* **2008**, *19*, 125606.
(9) Mou, F. Z.; Guan, J. G.; Xiao, Z. D.; Sun, Z. G.; Shi, W. D.; Fan, X. A. *J. Mater. Chem.* **2011**, *21*, 5414–5421.
(10) Cao, S. W.; Zhu, Y. J. *J. Phys. Chem. C* **2008**, *112*, 6253–6257.
(11) Tanboonchuy, V.; Hsu, J. C.; Grisdanurak, N.; Liao, C. H. *Environ. Sci. Pollut. Res.* **2011**, *18*, 857–864.
(12) Cao, H. Q.; Wang, G. Z.; Zhang, L.; Liang, Y.; Zhang, S. C.; Zhang, X. R. *Chemphyschem* **2006**, *7*, 1897–1901.
(13) Tang, B.; Wang, G. L.; Zhuo, L. H.; Ge, J. C.; Cui, L. J. *Inorg. Chem.* **2006**, *45*, 5196–5200.
(14) Liu, B. J.; Wang, D. F.; Li, H. Y.; Xu, Y.; Zhang, L. *Desalination* **2011**, *272*, 286–292.
(15) Tang, W. S.; Li, Q.; Li, C. F.; Gao, S. A.; Shang, J. K. *J. Nanopart. Res.* **2011**, *13*, 2641–2651.
(16) Liao, X. H.; Zhu, J. J.; Zhong, W.; Chen, H. Y. *Mater. Lett.* **2001**, *50*, 341–346.
(17) Li, S. Z.; Hong, Y. C.; Uhm, H. S.; Li, Z. K. *Jpn. J. Appl. Phys.* **2004**, *43*, 7714–7717.
(18) Hwang, J. Y.; Shi, S.; Xu, Z.; Peterson, K. W. *Chem. Eng. Commun.* **2006**, *193*, 1586–1591.
(19) Almeida, T. P.; Fay, M.; Zhu, Y. Q.; Brown, P. D. *J. Phys. Chem. C* **2009**, *113*, 18689–18698.
(20) Cao, M. H.; Liu, T. F.; Gao, S.; Sun, G. B.; Wu, X. L.; Hu, C. W.; Wang, Z. L. *Angew. Chem., Int. Ed.* **2005**, *44*, 4197–4201.
(21) Wang, S. B.; Min, Y. L.; Yu, S. H. *J. Phys. Chem. C* **2007**, *111*, 3551–3554.
(22) Huang, H.; Sithambaram, S.; Chen, C. H.; Kithongo, C. K.; Xu, L. P.; Iyer, A.; Garces, H. F.; Suib, S. L. *Chem. Mater.* **2010**, *22*, 3664–3669.
(23) Hu, X. L.; Yu, J. C.; Gong, J. M.; Li, Q.; Li, G. S. *Adv. Mater.* **2007**, *19*, 2324–2329.
(24) Hu, X. L.; Yu, J. C. *Adv. Funct. Mater.* **2008**, *18*, 880–887.
(25) Katsuki, H. *J. Am. Ceram. Soc.* **2001**, *84*, 2313–2317.
(26) Teng, Y.; Sakurai, H.; Ueda, A.; Tobayashi, T. *Int. J. Hydrogen Energy* **1999**, *24*, 355–358.
(27) Zhou, M.; Gao, Y.; Wang, B.; Rozynek, Z.; Fossum, J. O. *Eur. J. Inorg. Chem.* **2010**, 729–734.
(28) Yin, H.; Feng, X. H.; Qiu, G. H.; Tan, W. F.; Liu, F. *J. Hazard. Mater.* **2011**, *188*, 341–349.
(29) Wang, S. B.; Peng, Y. L. *Chem. Eng. J.* **2010**, *156*, 11–24.
(30) Simeonidis, K.; Gkinisa, Th.; Tresintsi, S.; Martinez-Boubeta, C.; Vourlias, G.; Tsiaoussis, I.; Stavropoulos, G.; Mitrakas, M.; Angelakeris, M. *Chem. Eng. J.* **2011**, *168*, 1008–1015.
(31) Ai, Z. H.; Lu, L. R.; Li, J. P.; Zhang, L. Z.; Qiu, J. R.; Wu, M. H. *J. Phys. Chem. C* **2007**, *111*, 7430–7436.
(32) Song, L. M.; Zhang, S. J.; Chen, B.; Ge, J. J.; Jia, X. C. *Colloids Surf., A* **2010**, *360*, 1–5.
(33) Kruk, M.; Jaroniec, M. *Chem. Mater.* **2001**, *13*, 3169–3183.
(34) Li, J. H.; Wang, R. H.; Hao, J. M. *J. Phys. Chem. C* **2010**, *114*, 10544–10550.
(35) Ali, A. H.; Zaera, F. *J. Mol. Catal. A: Chem.* **2002**, *177*, 215–235.
(36) Zaera, F. *Chem. Rec.* **2005**, *5*, 133–144.
(37) Yang, W.; Li, Q.; Gao, S.; Shang, J. K. *J. Mater. Sci.* **2011**, *46*, 5851–5858.
(38) Zhong, L. S.; Hu, J. S.; Wan, L. J.; Song, W. G. *Chem. Commun.* **2008**, *44*, 1184–1186.